

Probing Hard Scattering Processes via Multiple Weak Gauge Boson Production at the Future Colliders

Ijaz Ahmed,^{1,*} M. S.Amjad,^{2,†} and Jamil Muhammad^{3,‡}

¹*Federal Urdu University of Arts, Science and Technology, Islamabad, Pakistan*

²*National University of Technology, Islamabad, Pakistan*

³*Sang-Ho College of Education, Konkuk University, Seoul 05029, Korea*

(Dated: December 5, 2025)

Abstract

One of the possible ways to detect the new physics phenomena particles is to investigate the weak gauge boson production as a result of hadron-hadron scattering. This study comprises the production of multiple weak gauge bosons as a result of hard scattering between the proton-proton beams at multi-TeV energies and integrated luminosity $\mathcal{L} = 3000 \text{ fb}^{-1}$. The effective production cross-sections for pair, triple, and quartic scattering mechanisms have been computed as a function of \sqrt{s} . The center of mass energy has been varied from 8 TeV to 100 TeV to encompass the future collider capabilities. Out of all the studied processes, the triple scattering process $W^+W^-W^+$ has been chosen as the signal process based on the dominant cross-section. The background channels ZZZ , $ZZZZ$, W^-ZZ , W^+ZZ , W^+W^-Z , W^+W^-ZZ , $W^+W^-W^+W^-$, having comparatively lower cross-sections, have been selected from possible scattering mechanisms to investigate the effect of higher luminosity on the low production cross-section processes. We have investigated the different decay modes. For both lepton and hadron-specific decays of W and Z, the cumulative efficiencies for each signal and background process have been computed. In this study, we have successfully demonstrated an effective methodology for background suppression by systematically optimizing the signal-to-background ratio. The results indicate that, despite lower cross-sections for higher-order scattering, the distinct kinematic features enable effective signal isolation at future colliders.

PACS numbers: 12.15.Ji, 13.85.-t, 14.70.Fm, 14.70.Hp

Keywords: Gauge Bosons, Hard Scattering, Future Collider, Scattering mechanism, Background channels

*Electronic address: ijaz.ahmed@fuuast.edu.pk

†Electronic address: sohailamjad@nutech.edu.pk

[‡]Electronic address: mjamil@konkuk.ac.kr

I. INTRODUCTION

The Standard Model of particle physics (SM) gives a sufficient explanation of three basic particle interactions. It encompasses two additional theories, electroweak theory [1] and quantum chromodynamics (QCD) [2]. However, there are multiple unanswered questions, including gravity [3], dark matter, matter-antimatter asymmetry, sterile neutrino oscillations [4], etc. Therefore, it is considered incomplete [5]. An endeavor to find New Physics or Physics beyond the Standard Model has been going on for multiple decades. A possible avenue to discover the new particles is through multiple weak gauge boson production and by studying the scattering of bosons produced as a result of hadron-hadron collisions [6]. In this recent study, we address this aspect, which has not been frequently studied, although there do exist some previous efforts in this regard, such as [7–10]. The specific objectives of this study are: (i) to compute and analyze the production cross-sections for pair, triple, and quartic gauge boson scattering across a broad energy spectrum (8 TeV to 100 TeV), (ii) to investigate the kinematic distributions of leptonic and hadronic decay modes to identify distinguishing features between signal and background processes, and (iii) to evaluate the signal significance and signal-to-background ratios at high luminosities ($\mathcal{L} = 3000 \text{ fb}^{-1}$) by applying optimized kinematic cuts.

Keeping such a scenario in mind, in this work we have examined the pair, the triple, and the quartic scatterings of the W and Z bosons. All these calculations are carried out using the standard model parameters. For all the possible scattering mechanisms, cross-sections are computed by varying collision energies from 8 TeV to 100 TeV. Particularly, the two decay modes, i.e., the hadronic and the leptonic decay of W and Z bosons, are considered. For lepton-specific decays, the W bosons decay as $W^{\pm} \rightarrow l^{\pm} \nu$ while the Z boson decays into a pair of lepton and anti-lepton $Z \rightarrow l^{-} l^{+}$. For the hadronic decay mode, both W and Z bosons decay into a pair of jets $Z/W^{\pm} \rightarrow jj$. The background processes have been suppressed using various kinematic cuts. For lepton-specific decays, we have plotted transverse momentum P_T , number of leptons N , missing transverse energy E_T , mass M_T , pseudorapidity η , and the azimuthal angle $\Delta\phi$. For these variables, the cuts are $P_T > 10$, $|\eta| < 3$. For the hadron specific decays we have also computed the reconstructed mass M and hadronic energy H_T . The applied cuts are, $P_T > 20$, $|\eta| < 3$, and $H_T > 600$. After applying each cut, the cumulative efficiencies for each decay mode and for each process are tabulated. Due to each

cut, the efficiency reduces compared to the previous value. In this final study, signal-to-background ratio S/B and other signal significance S/\sqrt{B} and $S/\sqrt{S+B}$ are also computed at the integrated luminosity $\mathcal{L} = 3000 \text{ fb}^{-1}$. For the hadronic decay, the significance ratio S/\sqrt{B} reduces from 13.69 to 11.82, whereas $S/\sqrt{S+B}$ gradually decreases from 10.19 to 8.46 after applying the cuts on various parameters.

II. ANALYSIS SETUP AND TOOLS

Event generation for pp collisions at $\sqrt{s} = 14 \text{ TeV}$ was performed using the Madgraph framework [11]. In the next step, such events are analyzed by using MadAnalysis [12]. The jet clustering and its reconstruction are carried out with the FastJet [13] interface. After that, the output is analyzed by the ROOT analysis package [14]. This investigation is separated into two sections, covering the leptonic and hadronic decay channels of the weak gauge bosons. In particular, the following weak boson production modes are analyzed:

- Double boson scattering
 - $pp \rightarrow ZZ$ and $pp \rightarrow W^+W^-$
 - For like-charged Gauge boson Pairs, jets are added to avoid Isospin violation.
 $pp \rightarrow W^+W^+jj$ and $pp \rightarrow W^-W^-jj$.
- Triple boson scattering
 - $pp \rightarrow ZZZ$, and $pp \rightarrow W^+W^-W^+$
 - $pp \rightarrow W^+W^-Z$, $pp \rightarrow W^+ZZ$, $pp \rightarrow W^-ZZ$, $pp \rightarrow ZZZ$
- Quartic boson scattering
 - $pp \rightarrow W^+W^-W^+W^-$ $pp \rightarrow ZZZZ$, and $pp \rightarrow W^+W^-ZZ$

In addition, we are going to investigate and analyze the production modes of the parameters like production cross section as a function of center of mass energy $\sigma(\sqrt{s})$, pseudorapidity η , lepton multiplicity $N(\text{lepton})$ (for leptonic decays only), Lepton transverse momentum p_T (for leptonic decays only), lepton transverse mass M_T (for leptonic decays only), missing transverse energy E_T (for leptonic decays only), hadronic energy H_T (for hadronic decays only) and invariant mass of jets (for hadronic decays only)

III. RESULTS AND DISCUSSION

The production cross-sections governing pair and triple scattering mechanisms exhibit rapid scaling behavior, rising sharply as a direct function of the increasing center-of-mass energy. However, after 30 TeV, the increase is not very significant, and it tends to become constant. The highest production is for the oppositely charged W pairs, followed by Z pairs, and then, as expected, like-charge weak bosons cross-section. This scenario can be viewed in Figure 1. It is worth noting that the change in behavior after 30 TeV is very similar for all the scattering bosons.

The lepton-specific decays, as mentioned earlier, are of two types for each weak boson. W

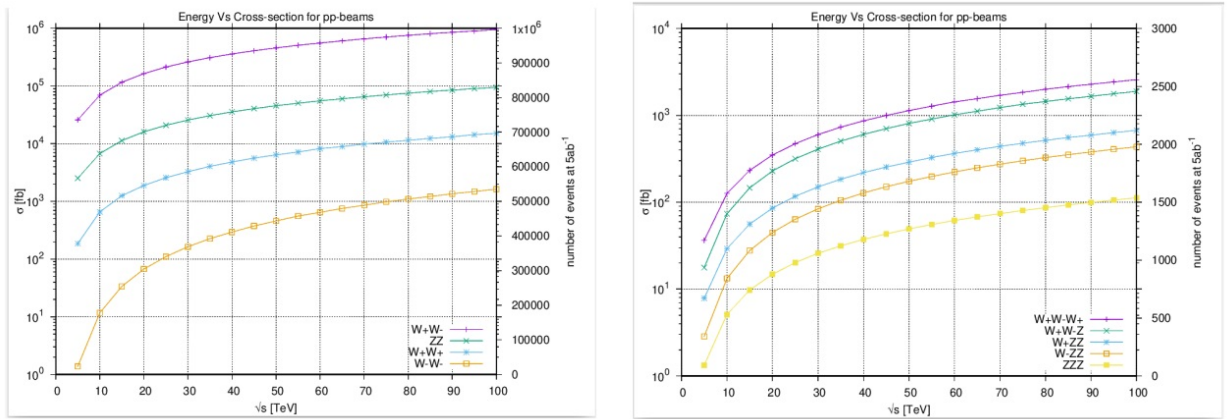


FIG. 1: The dependence of the production cross section on the center of mass energy is shown for double (left) and triple (right) boson scattering.

bosons typically decay into a lepton paired with its associated neutrino, whereas Z bosons decay into a pair of leptons with opposite charges. We analyze the transverse momentum and mass of the leptons that are generated from these decays and present them in Figure 2. We can see that the triple boson scattering where only one W is present with two Z bosons behaves a bit differently as compared to the other modes. Furthermore, the overall trend for both of these variables remains the same for the different kinds of scattering over the range of p_T and M_T . However, we do observe a difference in the peak for different scattering channels, where the reconstructed momentum peak seems to be lower for the quartic scatterings.

Our investigation proceeds to the analysis of missing transverse energy. This kinematic

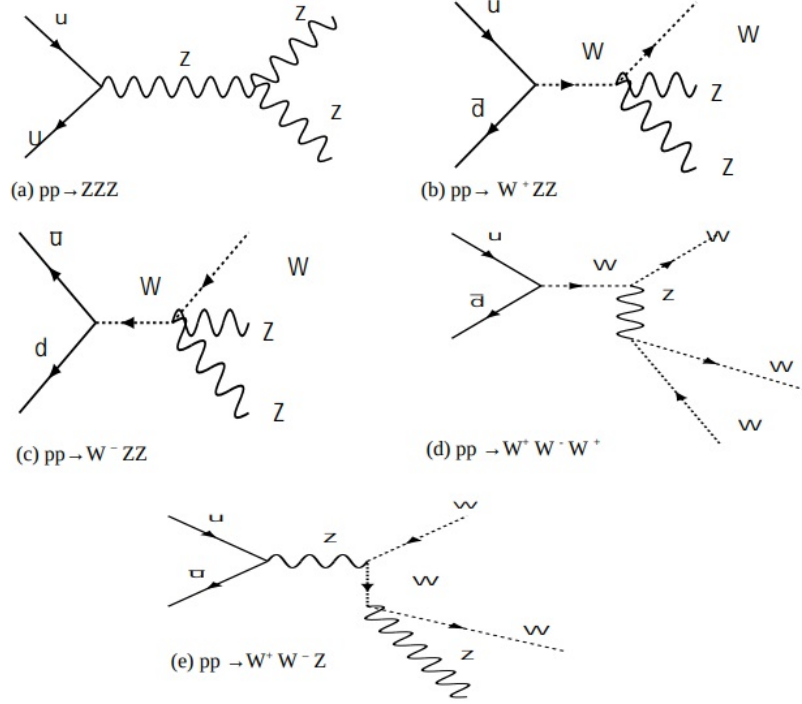


FIG. 2: A view of the possible Feynman diagrams for multiple gauge boson production.

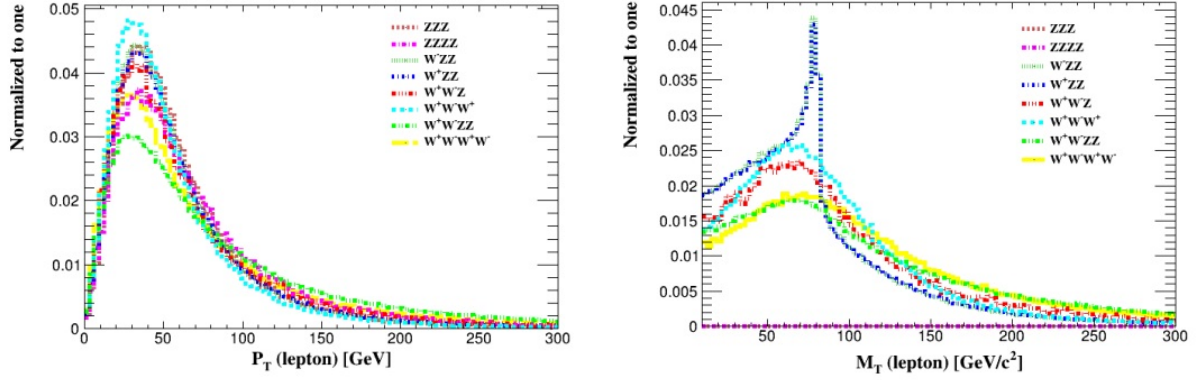


FIG. 3: The transverse momentum p_T (left) and mass M_T (right) are shown for the lepton-specific decay modes.

signature arises from the emission of invisible neutrinos during the leptonic decay channels of charged W bosons, a process that is schematically illustrated in Figure 3. We observe the variation in pattern for the reconstructed E_T based on the number and type of bosons being analyzed.

The single W channels have a clear peak with the right tail, while the two or more W boson channels show a larger spread of neutrino energy. Figure 4, illustrates the missing

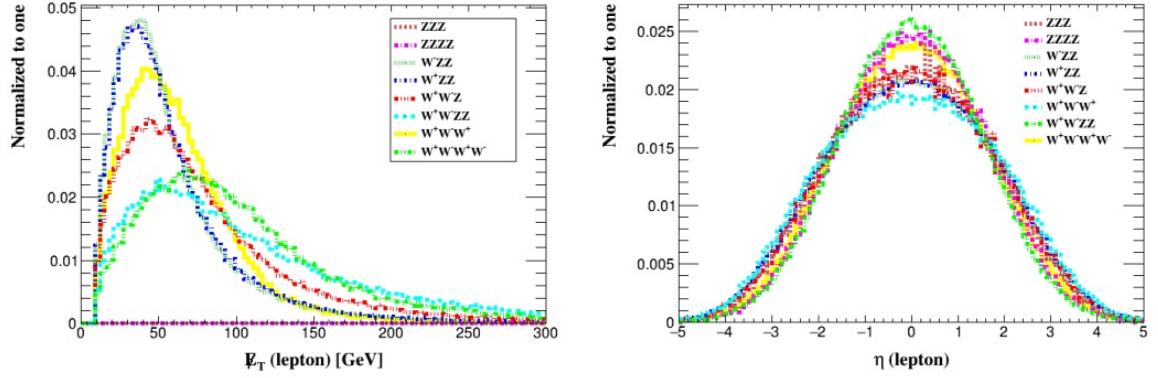


FIG. 4: The missing transverse energy (left) and pseudorapidity for the single leptonic decay of the W bosons.

transverse energy (E_T) distribution for the single leptonic decay of the W bosons. As shown in Figure 4, the distribution follows a Gaussian-like trajectory with a prominent peak in the 30–60 GeV range, corresponding to the typical neutrino momentum. The differing peak heights and tail extensions indicate that quartic and triple scattering processes exhibit broader energy dispersion compared to pair production, a feature that aids in distinguishing complex multi-boson events from simpler backgrounds.

A. Pair of Weak Gauge Boson Production

Whenever the multiple partons interact, they exchange momentum and reach higher energy levels because the maximum flux of partons is observed. The probability of Parton Pair Scattering with hadron interactions was anticipated a long time ago [15–17]. However, at CERN, the AFS collaboration provided evidence for double scattering in proton-proton collisions [18, 19]. Moreover, this process was observed at the Fermi lab by Collider Detector by considering the final states of the particles [20]. If two or more parton pairs scatter independently in hadronic collisions, multiple parton scattering occurs [21]. This double scattering examines the correlation between partons and hadrons in the transverse plane by providing more information about the hadronic structure. The parton-parton correlation can be neglected if the scattering event is parameterized by high energy. The dependence of the production cross-section on the center-of-mass energy was evaluated for the scattering of weak gauge boson pairs.

Table I displays the cross-sections for the weak gauge boson pair using the different energy ranges. For each process cross-section is calculated between the energy range 8 TeV and 100 TeV. The expected error is also computed for each process. FD represents the possible Feynman diagrams for each process. However, jets are added to avoid isospin violation for like-charged Gauge boson Pairs. Further, the jets are the light quarks too. In particle physics, a jet is generally produced by the hadronization of quarks or gluons by making a narrow cone.

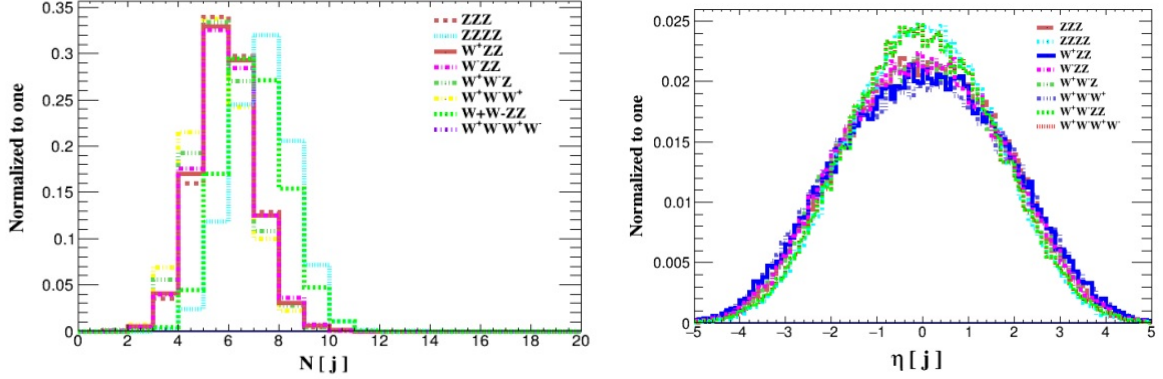


FIG. 5: (left) A distribution of jet multiplicity for hadron-specific decay of all gauge bosons. (Right) The plot shows the pseudorapidity distribution of jets for signal and all background processes.

TABLE I: The cross-sections for pair weak gauge bosons for various energy ranges.

Process	8 TeV $\sigma[pb] \pm error$	14 TeV $\sigma[pb] \pm error$	27 TeV $\sigma[pb] \pm error$	100 TeV $\sigma[pb] \pm error$	F.D
ZZ	4.803 ± 0.0114	10.3 ± 0.122	23.02 ± 0.0053	98.36 ± 0.0237	10
W^+W^-	34.15 ± 0.080	64.62 ± 0.168	154.3 ± 0.292	637.2 ± 1.451	10
$W^+W^- jj$	0.08206 ± 0.002	0.2153 ± 0.0006	0.584 ± 0.021	2.9 ± 0.120	11
$W^+W^- jj$	0.0307 ± 0.0005	0.09548 ± 0.002	0.3017 ± 0.007	2.05 ± 0.006	11

B. Triple Parton Scattering of Weak Gauge Boson

In the standard model [22], the approximations of cross-section and cms energy for three weak gauge bosons have been performed. Table II shows the cross-sections along with vary-

TABLE II: The cross-sections along with varying energy for the triple scattering mechanism.

Process	8 TeV $\sigma[pb] \pm error$	14 TeV $\sigma[pb] \pm error$	27 TeV $\sigma[pb] \pm error$	100 TeV $\sigma[pb] \pm error$	F.D
ZZZ	0.0042 \pm 0.0009	0.01028 \pm 0.005	0.02672 \pm 0.0006	0.1357 \pm 0.003	42
$W^- ZZ$	0.0357 \pm 0.006	0.014 \pm 0.005	0.02966 \pm 0.005	0.162 \pm 0.0032	28
$W^+ ZZ$	0.0075 \pm 0.008	0.01844 \pm 0.005	0.0499 \pm 0.0001	0.227 \pm 0.0006	36
$W^+ W^- W^+$	0.03404 \pm 0.008	0.07877 \pm 0.022	0.1922 \pm 0.006	0.9201 \pm 0.001	40

TABLE III: The cross-sections for the quartic scattering mechanism along with varying energy.

Process	8 TeV $\sigma[pb] \pm error$	14 TeV $\sigma[pb] \pm error$	27 TeV $\sigma[pb] \pm error$	100 TeV $\sigma[pb] \pm error$	F.D
ZZZZ	$5.88 \times 10^{-6} \pm 0.001$	$1.87 \times 10^{-5} \pm 0.004$	$6.03 \times 10^{-5} \pm 0.0001$	$3.8 \times 10^{-3} \pm 0.00015$	192
$W^+ W^- ZZ$	$1.1 \times 10^{-4} \pm 0.0006$	$4.2 \times 10^{-4} \pm 0.0001$	$4.3 \times 10^{-4} \pm 0.0002$	0.0106 ± 0.0003	426
$W^+ W^- W^+ W^-$	$1.5 \times 10^{-4} \pm 0.001$	$4.9 \times 10^{-4} \pm 0.0001$	$1.6 \times 10^{-3} \pm 0.0005$	0.0103 ± 0.00042	592

ing energy for the triple scattering mechanism. For each process cross-section is calculated between energy ranges 8 TeV to 100 TeV. The expected error is also computed for each process. In this Table, FD represents the possible Feynman diagrams for each process.

Table III displays the cross-sections for the quartic scattering mechanism along with varying energy at cms. The cross-sections for the quartic scattering mechanism are the processes along with the errors that are computed. All these calculations showed that by increasing the center of mass energy, the cross-section of various scattering mechanisms increases rapidly. A sharp increase can be seen graphically.

C. Pseudorapidity

It is the angle between the particle and the beam axis [23], [24]. It has one-to-one correspondence with the polar angle θ . It can be expressed as:

$$\eta = -\ln[\tan(\theta/2)]$$

where θ is the angle between the three components of momentum and the positive beam axis. The particles with $\eta = 0$ are along the beam axis, while the particles having large pseudorapidity are lost. Kinematic cuts $|\eta| < 3$ are used to suppress the background. Figure 5 displays the pseudorapidity for leptonic decays.

D. Multiplicity

Multiplicity refers to the number of particles present in a specific process for a specific center of mass energy in a certain decay [25]. Here, in Figure 5, the lepton multiplicity is plotted. W and Z bosons have extremely short lifetimes of approximately $\sim 10^{-25}$ s, decaying into quarks and leptons with distinct branching fractions. Specifically, the W boson decays into a charged lepton-neutrino pair about 33% of the time, with the remaining 67% resulting in hadronic states. In contrast, the Z boson yields hadrons 70% of the time, neutrinos 20% of the time, and charged lepton pairs approximately 10% of the time. For both bosons, the hadronic decay modes are notably challenging to identify due to the overwhelming dijet background, which is orders of magnitude higher. Table IV depicts the cumulative efficiencies for each background and signal processes for the lepton-specific decay at cms energy 14 TeV. The calculated cross-sections for both signal and background events are summarized in the Table. Additionally, we define P_T as the transverse momentum associated with the leptonic decays of W and Z bosons, imposing a kinematic threshold of $P_T > 10$. As neutrinos remain unaffected by some interactions, there exists missing transverse energy for which the cuts $E_T > 80$ are applied. The effective cross-sections for Z boson triple and quartic scattering are very low, so applying the kinematic cuts on transverse momentum, the numbers for efficiency reduce, whereas by applying missing transverse energy and pseudorapidity cuts, their values almost reduce to zero. The rest of the processes show variation in efficiencies by applying kinematic cuts. Upon applying kinematic cuts of $P_T > 10$, $E_T > 80$ and $|\eta| < 3$, we calculated the significance and S/B ratios, which are presented in Table V.

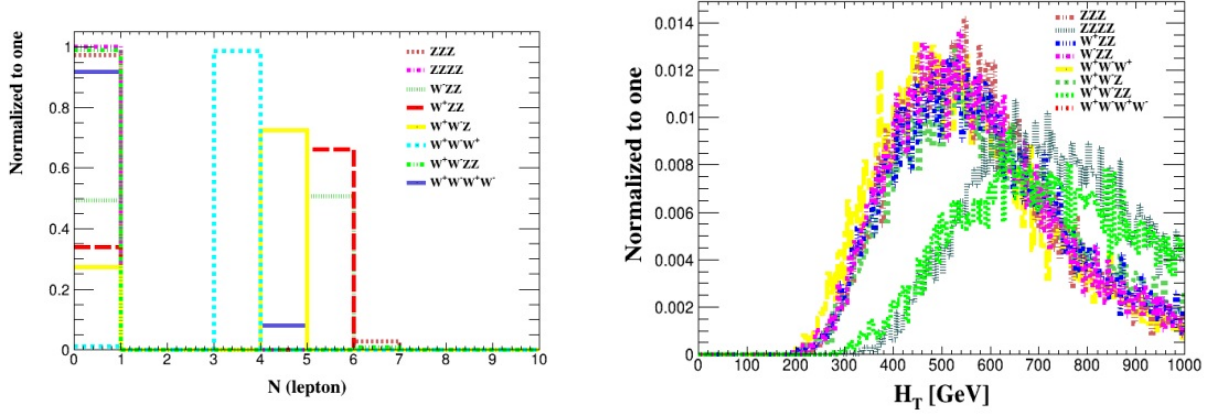


FIG. 6: The Lepton multiplicity for various Decays of weak gauge bosons at the left side, while the view of the distribution of the Hadronic Energy (HT) in the Hadron-specific decay at the right side.

TABLE IV: The cumulative efficiencies for each background and signal processes for lepton-specific decay at cms energy 14 TeV.

Triple Boson Scattering					
	ZZZ	W^-ZZ	W^+ZZ	W^+W^-Z	$W^+W^-W^+$
$\sigma[pb]$	3.1×10^{-6}	1.03×10^{-5}	1.96×10^{-5}	3.0×10^{-4}	8.4×10^{-3}
$P_T > 10$	0.2 ± 0.24	$0.50^{-5} \pm 0.15$	0.6 ± 0.11	0.96 ± 0.1	0.99 ± 0.004
Quartic Boson Scattering					
	$ZZZZ$	W^+W^-ZZ	$W^+W^-W^+W^-$		
$\sigma[pb]$	4.9×10^{-10}	9.32×10^{-9}	1.28×10^{-8}		
$P_T > 10$	$4 \times 10^{-5} \pm 0.32$	$9 \times 10^{-4} \pm 0.3$	0.081 ± 0.24		

E. Hadronic decays

Since W and Z bosons possess hadronic decay channels, we reconstructed the invariant masses of the resulting jets to analyze these specific modes. The signal and the background processes are selected, and the significance for each process is tabulated. In the analysis of hadronic decays, we designated the $W^+ W^- W^+$ channel as the signal, treating all other interactions as background. The corresponding cross-sections for these processes are

presented in the table. The parameters for the hadronic decays are also plotted. In case of the hadron-specific decays, ‘jets’ are included, that is, the narrow cone of the hadrons produced as a result of the hadronization.

The other observables are also plotted for the hadron-specific decays. Instead of missing transverse energy, the hadronic energy distribution is plotted as shown in Figure 6. Similarly, the jet multiplicity $N(j)$, which shows the number of jets present in each process, is also computed as shown in Figure 6(a). Moreover, the pseudorapidity of jets for hadron-specific decay is estimated and presented in Figure 6(b).

IV. INVARIANT MASS

The invariant mass is generated with the possible jet pairs. It can be computed using the chi-square method [26, 27].

$$\chi^2 = \frac{\Sigma(W_{reci} - 80.5)}{\sigma_{jets}}$$

We calculate the reconstructed invariant mass using the expression below:

$$m_{inv}^2 = E^2 + |P|^2$$

The plots for the invariant mass distributions are presented in Figure 7.

Table V, shows the signal significance ratios of signals and backgrounds for leptonic decay. While Table VI presents the cumulative efficiencies for both signal and background events. These results reflect the application of specific selection cuts designed to minimize background channels. As detailed in Table V, the impact of kinematic cuts on the signal-to-background ratio is significant. We observe that applying the $P_T > 10$ GeV cut yields an S/B ratio of approximately 2.19. While stricter cuts on Missing $E_T(> 80)$ and pseudorapidity ($|\eta| < 3$) result in a decrease in the raw signal count to 1966.8 events, the statistical significance S/\sqrt{B} remains robust at approximately 59. This confirms that even after rigorous background suppression, the signal remains statistically observable at an integrated luminosity of 3000 fb^{-1} .

A close look at Table VII shows that the selection cut of transverse momentum of jets $P_T > 20$ has been applied. For the hadronic energy, we have also applied a cut that is $H_T < 600$. By applying various kinematic cuts, the value for the S/B ratio decreases (as tabulated in

Table VII) as one process is chosen to be the signal and the rest of them as backgrounds so it is important to compute their signal-to-background ratio. By applying cuts, the signal-to-background ratio (S/B) reduces. After application of various cuts, the rest of the signal significance ratios also reduce. For instance, here in this Table, when no cuts are applied, the signal is 234. However, after applying the cut, its value reduces to 145.64. The significance ratio S/\sqrt{B} reduces from 13.69 to 11.82, whereas $S/\sqrt{S+B}$ gradually decreases from 10.19 to 8.46 after applying cuts on various parameters. The significance plots are also constructed, and signal-to-background ratios are computed for each process at the luminosity of 3000 fb^{-1} .

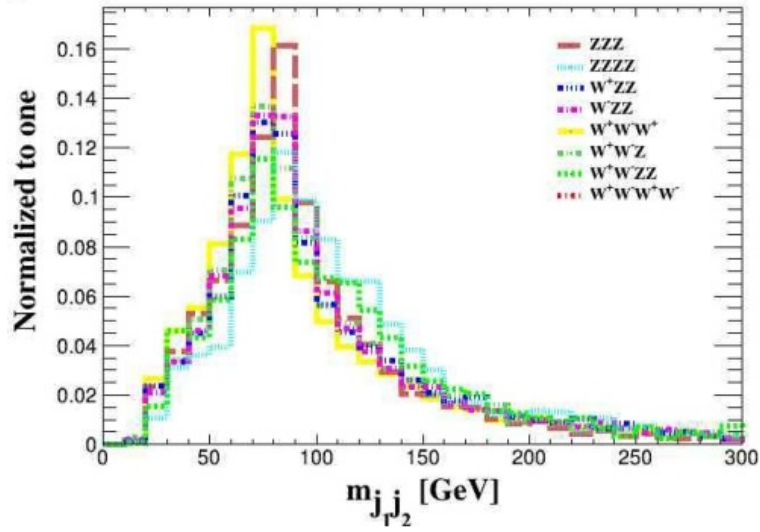


FIG. 7: The view of the invariant mass distribution of jet pair.

TABLE V: The signal significance ratios of signals and backgrounds for leptonic decays at $L \sim 3000 \text{ fb}^{-1}$ and $\sqrt{s} = 14 \text{ TeV}$.

Cuts	Signal	Background	S/B	S/\sqrt{B}	$S/\sqrt{S+B}$
No cuts	8437.41 ± 7.12	3331.2 ± 2.6	2.5328 ± 0.002	146.1878 ± 0.0023	77.776 ± 0.043
$P_T > 10$	6297.7 ± 40.3	2876.8 ± 8.9	2.1891 ± 0.020	117.41611 ± 0.001	65.749 ± 0.285
$E_T > 80$	1968.8 ± 38.9	1105.5 ± 26.9	1.7809 ± 0.055	59.21308 ± 0.0072	35.508 ± 0.501
$ \eta < 3$	1966.8 ± 38.9	1105.2 ± 26.9	1.7796 ± 0.055	59.16244 ± 0.0072	35.486 ± 0.501

TABLE VI: The cumulative efficiency for the hadronic decay of weak gauge bosons.

Triple Boson Scattering					
	ZZZ	W^-ZZ	W^+ZZ	W^+W^-Z	$W^+W^-W^+$
$\sigma[pb]$	0.00155	0.00192	0.00367	0.0218	0.0218
$P_T(j) > 20$	0.13 ± 0.08	0.14 ± 0.08	0.99 ± 0.01	0.99 ± 0.01	0.99 ± 0.004
Quartic Boson Scattering					
	ZZZZ	W^+W^-ZZ	$W^+W^-W^+W^-$		
$\sigma[pb]$	1.58×10^{-6}	0.00011	0.00011		
$P_T(j) > 20$	0.31 ± 3.6	0.41 ± 0.47	0.4 ± 0.47		

TABLE VII: The signal-to-background ratio for each process in the hadronic decay.

Cuts	Signal	Background	S/B	S/\sqrt{B}	$S/\sqrt{S+B}$
No cuts	234.0	291.0	0.0804	13.7	10.2
$N(j) \geq 6$	232.95 ± 1.14	289.20 ± 1.44	0.80526 ± 0.0056	13.69621 ± 0.0017	10.1937 ± 0.0413
$ \eta (j) < 3$	232.86 ± 1.18	289.19 ± 1.47	0.80521 ± 0.0057	13.69310 ± 0.0017	10.1915 ± 0.0427
$H_T < 600$	145.64 ± 7.42	150.25 ± 8.51	0.9693 ± 0.0738	11.882 ± 0.019	8.467 ± 0.347

V. CONCLUSION

The primary scope of this research was to scrutinize the generation of multiple weak gauge bosons arising from high-energy proton-proton interactions. This analysis is conducted within the projected experimental environment of the Large Hadron Collider (LHC), assuming a center-of-mass energy of $\sqrt{s} = 14$ TeV and a target integrated luminosity of 3000 fb^{-1} . The calculations of cross-sections at the center of mass energy 100 TeV for future colliders are also estimated. In this analysis, $W^+W^-W^+$ is assumed as a signal and the rest of them as the background channels. We have successfully characterized the kinematic behaviors of these channels, particularly highlighting the discriminating power of missing transverse energy and invariant mass distributions.

We have summarized that our finalized plots for each variable are in good agreement with

the actual values. The analytical framework presented herein is designed to serve as a pivotal resource for future investigations into the production of multiple weak gauge bosons within the Standard Model context. Based on current simulation data, the prospects for detection are highly encouraging; specifically, the chosen parameters for center-of-mass energy and integrated luminosity provide sufficient sensitivity to successfully observe all the theoretical scenarios hypothesized in this study. The calculated significances suggest that the $W^+W^-W^+$ channel will be accessible in the High-Luminosity LHC era, providing a vital test of the electroweak sector. Our results could be quite useful for researchers working in the field of multiple weak gauge bosons.

VI. ACKNOWLEDGMENT

VII. STATEMENTS AND DECLARATIONS

Funding The authors confirm that this work was conducted without any specific funding, grants, or financial assistance.

Competing Interests The authors declare that they have no competing interests, financial or otherwise .

-
- [1] Kibble, T. W. B. (2015, June). History of electroweak symmetry breaking. In *Journal of Physics: Conference Series* (Vol. 626, No. 1, p. 012001). IOP Publishing.
- [2] Aitchison, I. J., & Hey, A. J. (2012). *Gauge theories in particle physics: A practical introduction, Volume 2: Non-Abelian Gauge Theories: QCD and the electroweak theory* (Vol. 2). CRC Press.
- [3] De Andrade, V. C., & Pereira, J. G. (1997). Gravitational Lorentz force and the description of the gravitational interaction. *Physical Review D*, 56(8), 4689.
- [4] Kopp, J., Machado, P. A., Maltoni, M., & Schwetz, T. (2013). Sterile neutrino oscillations: the global picture. *Journal of High Energy Physics*, 2013(5), 1-52.
- [5] Johnson, J. R. (2021). Does a Theory of Everything Exist?. *Philosophy and Cosmology*, 26(26), 132-147.
- [6] Gallinaro, M., Long, K., Reuter, J., Ruiz, R., Bachas, D., Barak, L., ... & Szleper, M. (2020). Beyond the Standard Model in vector boson scattering signatures. *arXiv preprint arXiv:2005.09889*.
- [7] A. Oh, Measurements of multi vector boson production processes at the LHC. *Progress in Particle and Nuclear Physics* Volume 108, September 2019, 103708
- [8] Gunnellini, P. (2016). Study of double parton scattering using four-jet scenarios in proton-proton collisions at $\sqrt{s}=7$ TeV with the CMS experiment at the Large Hadron Collider (Doctoral dissertation, U. Hamburg, Dept. Phys.).
- [9] M. Y. Hussein, Multiple Weak Gauge Boson production at the LHC as a probe of hard scattering processes, *Quark Confinement and the Hadron Spectrum V*, pp. 484-488 (2003)
- [10] D.A. Morris, Prospects for Multiple Weak Gauge Boson Production at Supercollider Energies, *arXiv:hep-ph/9308326*
- [11] J. Alwall, *et al.* The automated computation of tree-level and next-to-leading order differential cross sections, and their matching to parton shower simulations. *JHEP* Volume 2014, article number 79, (2014)
- [12] Eric Conte *et al.* MadAnalysis 5, a user-friendly framework for collider phenomenology. *Computer Physics Communications*, Volume 184, Issue 1, January 2013, Pages 222-256
- [13] Matteo Cacciari, FastJet: a code for fast k_t clustering, and more. *arxiv.org/abs/hep-*

- [14] Rene Brun and Fons Rademakers, ROOT - An Object-Oriented Data Analysis Framework, Proceedings AIHENP'96 Workshop, Lausanne, Sep. 1996, Nucl. Inst. & Meth. in Phys. Res. A 389 (1997) 81-86. DOI: <https://zenodo.org/records/3895860>
- [15] Edgar Huayra, Emmanuel G. de Oliveira and Roman Pasechnik, Probing double parton scattering via associated open charm and bottom production in ultraperipheral pA collisions, Theoretical Physics, Published: 26 October 2019 Volume 79, article number 880, (2019)
- [16] Jeppe R. Andersen, Pier Francesco Monni, Luca Rottoli, Gavin P. Salam, Alba Soto-Ontoso, Exploring high-purity multi-parton scattering at hadron colliders, arXiv:2307.05693v2 [hep-ph] 17 May 2024. Link at: <https://arxiv.org/html/2307.05693v2>
- [17] Tomas Kasemets, Double parton scattering - a tale of two partons, PhD Thesis, University of Hamburg, 2013. <https://inspirehep.net/files/e1864145becde25d32d7fa61339727c1>
- [18] D. Cockerill et al, Performance of the AFS-Vertex Detector at the CERN ISR, 1981 Phys. Scr. 23 649 <https://iopscience.iop.org/article/10.1088/0031-8949/23/4B/007/pdf>
- [19] O. Botner, V. Burkert, D. Cockerill et al., "Performance of the AFS vertex detector at the CERN ISR", Nuclear Instruments and Methods in Physics Research, Volume 196, Issue 1, 1 May 1982, Pages 315-318. <https://www.sciencedirect.com/science/article/abs/pii/0029554X82906619>
- [20] The CDF (Collider Detector experiment at Fermilab), Batavia IL 60510-5011, USA Linked <https://cdf.fnal.gov/about.html>
- [21] Abramowicz, H., Bartalini, P., Bähr, M., Cartiglia, N., Ciesielski, R., Dobson, E., & Wijeratne, P. (2013). Summary of the workshop on multi-parton interactions (MPI@ LHC 2012). arXiv preprint arXiv:1306.5413.
- [22] Hanna Grönqvist, "Particle physics models with four generations", "The Standard Model, Chapter- 2"; PhD Thesis, Institute of Physics University of Helsinki, Finland 2012 <https://inspirehep.net/files/394b77992cfc57326d34bdccf0c0ef2f>
- [23] E. Daw, "Lecture 7- Rapidity and Pseudorapidity", March 2012. https://www.hep.shef.ac.uk/edaw/PHY206/Site/2012_course_files/phy206rlec7.pdf
- [24] Zhijin Jiang, Yan Huang, Haili Zhang, Yu Zhang, "Hydrodynamic description of pseudorapidity distributions of charged particles in p-p collisions at center-of-mass energies from 23.6 GeV to 7 TeV", Chinese Journal of Physics, Volume 54, Issue 3, June 2016, Pages 371-378.

- [25] Duncan A. Morris, “prospects for multiple weak gauge boson production at supercollider energies”, UCLA 93/TEP/30, August 1993. <https://arxiv.org/pdf/hep-ph/9308326>
- [26] ”Chi-Square - Sociology 3112 - Department of Sociology - The University of Utah”. soc.utah.edu. Retrieved 2025-01-03.
- [27] Chi-Square Testing, Statistics in Medicine (Second Edition), 2006. <https://www.sciencedirect.com/topics/mathematics/chi-square-testing>